electronics

Article

Leakage Fault Diagnosis of Two Parallel Cylinders in Pneumatic System with a Minimal Number of Sensors

Hongwei Zhu, Zhiwen Wang *, Hu Wang, Zecheng Zhao and Wei Xiong *

Department of Mechanical Engineering, Dalian Maritime University, Dalian 116026, China; zhuhongwei722@dlmu.edu.cn (H.Z.); huwang@dlmu.edu.cn (H.W.); zzcmx@dlmu.edu.cn (Z.Z.)
* Correspondence: wzw@dlmu.edu.cn (Z.W.); xiongwei@dlmu.edu.cn (W.X.)

Abstract: The low investment cost is one of the core competitiveness advantages of pneumatic power systems. With increasingly pressing intelligent manufacturing, it is meaningful to investigate the feasibility of implementing fault diagnoses of pneumatic systems with a minimal number of low-cost sensors. In this study, a typical pneumatic circuit with two parallel-installed cylinders is taken as an example. The pressure, flow rate, and exergy data collected from upstream sensors are used for diagnosing the leakage faults in two downstream cylinders with the help of different machine learning methods. The features of data are extracted with stacked auto-encoders. Gaussian process classifier, support vector machine, and k-nearest neighbor are used for classifying faults. The results show that it is feasible to detect and diagnose downstream multi-faults with one or two upstream sensors. In terms of the working conditions presented in this study, the average accuracy of diagnosis with exergy data is the highest, followed by flow-rate data and pressure data. The support vector machine performs the best among the three machine learning methods.

Keywords: pneumatics; fault diagnosis; exergy; machine learning; compressed air; support vector machine

Citation: Zhu, H.; Wang, Z.; Wang, H.; Zhao, Z.; Xiong, W. Leakage Fault Diagnosis of Two Parallel Cylinders in Pneumatic System with a Minimal Number of Sensors. *Electronics* **2023**, *12*, 3261. https://doi.org/10.3390/electronics12153261

Academic Editor: Wenxian Yang

Received: 30 May 2023
Revised: 14 July 2023
Accepted: 15 July 2023
Published: 29 July 2023

1. Introduction

Thanks to the metrics of simple structure, low initial investment cost, high reliability, environmental friendliness, long lifespan, etc., pneumatic systems are widely used in manufacturing systems [1,2]. Compared with the electrical, hydraulic, and mechanical power transmission systems, the pneumatic system lags in terms of fault diagnosis and energy efficiency. Intelligent manufacturing and green manufacturing are pushing more pressure on pneumatic power technologies. Although many attempts and investigations have been conducted in terms of fault detection and diagnosis in pneumatic systems and components, there is still a significant lack of feasibility in workshops when comprehensively considering the simplicity, economy, and accuracy.

In general, fault diagnosis methods of pneumatic systems can be categorized as experience-based, model-based, and data-based methods.

The traditional and most widely used method of fault diagnosis in pneumatic systems is the experience-based method. The experienced-based method is simple and easy to implement; nevertheless, the accuracy and efficiency of diagnoses are highly dependent on the experience of maintainers. Generally, the accuracy and efficiency of the experience-based method are very low. The experience-based fault diagnosis method in pneumatic systems was widely investigated a few decades ago. In the last two decades, the fault tree method and expert system were developed and expanded. Luo [3] used the fault tree analysis method to analyze the mechanism of pneumatic system faults for fault diagnosis. Wang et al. [4] studied the characteristics of faults in pneumatic product lines and proposed a fuzzy neural network fault diagnosis expert system. Guo et al. [5] proposed a design method for a knowledge-based diagnosis system, which added intelligent diagnosis and compensation functions to the real-time expert system for fault diagnosis in pneumatic systems. It was found that good diagnosis results can be obtained by combining the expert system with the neural network. Zhang et al. [6] proposed a fault diagnosis approach for pneumatic control valves based on a modified expert system by combining a particle swarm optimization (PSO) algorithm with expert rules. Actually, the effectiveness of the expert system is quite limited because it is difficult to acquire and represent the experience and knowledge of experts. Overall, the experience-based method is no longer fit for the modern market's requirements for efficient, fast, and low-cost production systems [7].

The premise of model-based fault diagnosis is to understand and utilize the relevant mathematical model to accurately describe the physical processes that affect the health status of the relevant components in systems [8]. One of the most important advantages of the model-based method is that it can model the random processes of the equipment's running state and can also be used to evaluate the current equipment state, estimate the remaining life of the equipment, and even achieve real-time prediction [9]. Theoretically, once the precise and reliable mathematical model is established, the model-based method should provide higher accuracy than other methods. However, it is generally too difficult to establish such an accurate and reliable mathematical model, especially for pneumatic systems with significant nonlinearity and coupling effects [10]. Generally, a large amount of historical data and experiments are required to determine the model's parameters that would change with changing working conditions. It is also a time-consuming and laborious process. In many cases, it is challenging to determine which prediction models are suitable for matching the historical faults identified through the collection and processing of different information using prior experiential knowledge [6]. This is especially true when considering the interaction, nonlinearity, randomness, and degradation. As a result, the accuracy of fault diagnosis with the rough model drops sharply. Establishing a precise mathematical model for a complex physical system in some actual states is difficult and impossible. Therefore, its application is limited and constrained, especially under variable working conditions and flexible production conditions. The strong coupling of compressed air pressure, flow rate, and temperature also makes model-based fault diagnosis for pneumatic systems more challenging [11].

In recent years, machine learning technology has been widely and successfully explored in many fields. Yin et al. [12] constructed a transformer fault diagnosis system using a Gaussian process classifier. Qi et al. [13] presented a fault diagnosis system for reciprocating compressors in the petroleum industry using big data and machine learning techniques. Experimental results indicated that the system could identify most potential faults with an accuracy rate exceeding 80%. Moosavian et al. [14] proposed a novel fault diagnosis scheme for the main journal bearing of an internal combustion engine based on power spectral density (PSD), k-nearest neighbor (KNN), and artificial neural network s(ANNs). Results demonstrated that reliable diagnoses of various faults could be achieved. Liu et al. [15] introduced a fault diagnosis method for rolling bearings that combines convolutional neural networks and transformers. The proposed method showed superior diagnostic performance in scenarios with limited data, intense noise, and varying operating conditions. Bai et al. [16] proposed an SSAE-SVM-based fault diagnosis method that enabled effective fault diagnosis of diesel engines in complex environments. Thus, machine learning could also provide a new and feasible way for the fault diagnosis of pneumatic systems. Many studies have been conducted in this field [17]. For example, Feng and Yang [18] proposed a fault diagnosis method for pneumatic actuators based on adaptive multi-kernel multi-classification relevance vector machines. With the DABLib software, a simulation model for pneumatic valve faults was established and data from various faults were simulated. Through machine learning technology, 18 types of faults were identified, and the recognition rate exceeded 95%. LEU et al. [19] proposed a fault diagnosis method for pneumatic circuits based on bidirectional LSTM. The method effectively diagnosed faults in the pneumatic circuit, achieving a fault diagnosis accuracy rate exceeding 95%. The data were obtained through simulation and were stable and of high quality. However, such high-quality, stable data usually do not exist in actual systems. Some signal acquisition is either unavailable or difficult to achieve in existing systems due to various operational and cost-related reasons. To conduct maintenance activities based on the state of the pneumatic actuator, Kovacs and Ko [20] proposed developing a signal processing method to monitor the machine state of the pneumatic actuator in real-time based on the actual data from the factory. They used the clustering signal to create a set of balanced training data, which was used to develop a supervised machine learning model. The machine learning technology analyzed the signal mode of the pneumatic actuator to identify and classify different machine states that may indicate abnormal behavior. Ertel et al. [21] believed that monitoring a single pneumatic component was too expensive and impractical, given that pneumatic production systems were unique and were usually designed for specific tasks. Therefore, they proposed to recognize and diagnose the pneumatic system's normal and abnormal working states using the single classification learning and nearest neighbor algorithm of machine learning technology. It should be noted that only the flow rate data collected in the manifold of the pneumatic system were used. They achieved excellent classification results without error. Demetgul et al. [22] evaluated the fault diagnosis performance of a combination of eight sensors and an artificial neural network (ANN) on Festo's teaching modular production system (MPS). They collected signals from eight sensors in the whole sequence and encoded 24 features of the data. By calculating the characteristics of the signal, they identified 11 faults. The results showed that the artificial neural network could be used to diagnose extremely complex pneumatic systems, but accurately diagnosing more faults required more sensors, which would mean higher costs. Therefore, they recommended keeping the number of failure modes below five to obtain a more reliable diagnosis. Li and Kao [23] used multi-resolution wavelets to decompose various sensor signals (such as pressure, flow, etc.) and used machine learning technology to diagnose leakage faults of pneumatic systems.

In general, in pneumatic systems, more types and numbers of sensors are needed for diagnosing multi-faults of multi-components, thereby significantly increasing the investment cost. This conflicts with the core competitiveness of pneumatic power technologies: low investment cost. Thus, it is meaningful to investigate the feasibility of implementing fault diagnoses of pneumatic systems with a minimal number of low-cost sensors.

Low energy efficiency is another remarkable defect of pneumatic systems. Usually, leakage accounts for about 10% to 40% of energy loss in pneumatic systems. Moreover, leakage could also lead to a drop in system pressure, reduce the functions of pneumatic components, shorten the service life, and further affect product quality [24]. Thus, leakage can be regarded as one of the most common faults and the main factor of energy waste in pneumatic systems. Thus, the leakage faults of pneumatic cylinders are investigated.

Pneumatic circuits with parallel-installed cylinders are popular in pneumatic systems. A complex task is generally completed via sequential operations of several pneumatic cylinders. The collaborative operations of parallel-installed cylinders could significantly enhance production efficiency and adapt to diverse work scenarios. They could achieve precise positioning and attitude adjustment through coordinated motion and synchronized control, thereby improving motion control accuracy and repeatability. Moreover, parallel cylinders can perform multiple tasks simultaneously, thereby enhancing work efficiency and shortening production cycles. Therefore, in this study, the parallel-installed double cylinders are selected as the objective. Machine learning methods are used to analyze data collected from a single measurement point upstream of the system to effectively diagnose multiple faults downstream.

Generally, the pressure signal and flow signal are the most commonly used factors for fault detection and diagnosis in pneumatic systems and have proven effective in many cases [25–27]. However, independent pressure signal and flow signal may not always provide satisfactory diagnostic performance, depending on specific systems and operating conditions. Therefore, in this study, a fused indicator, exergy, combining the features of pressure and flow, is selected.

The stacked auto-encoders (SAE) is used for extracting features from pressure, flow rate, and exergy signals. The extracted features are then input into machine learning models such as Gaussian process classifier (GPC), support vector machine (SVM), and k-nearest neighbor (KNN) to achieve learning, recognition, and classification of leakage faults. The study focuses on exploring the following three issues.

- Preliminarily prove the feasibility of fault diagnosis in pneumatic systems using a minimal number of low-cost sensors while ensuring high-precision results. This is important for achieving the balance between cost and performance.
- Compare the performance of fault diagnosis with flow, pressure, and exergy data and determine which data perform better.
- Compare three commonly used classifiers, GPC, SVM, and KNN, to determine the optimal classifier in this scenario.

The structure of this study is organized as follows. Section 2 details the experiment used in this study, including the experimental system, experimental data acquisition, and experiment settings. Section 3 introduces the methodology used in this study, including data preprocessing, machine learning methods, and fault diagnosis process. Section 4 analyzes and discusses the results from different perspectives. Finally, conclusions are drawn in Section 5.

2. Experiment

2.1. Experimental System

An experimental system is designed to diagnose and locate leakage faults in a circuit with two parallel-installed pneumatic cylinders, as shown in Figure 1. The main components and parameters are listed in Table 1. The extension and retraction of the piston rod of cylinder #1 and cylinder #2 are controlled by three-position five-way electromagnetic directional valve #1 and valve #2, respectively. The inlet and outlet of the rod-side of cylinder #1 and cylinder #2 are equipped with flow control valve #1 and flow control valve #2 to simulate the external leakage faults. Two sets of experiments were designed to simulate different working conditions, experiment I and experiment II, as shown in Table 2 and Figure 2. In experiment I, cylinder #1 and cylinder #2 are different types: cylinder #1 is A-type and cylinder #2 is B-type. The reversing frequency of directional control valves #1 and #2 is 0.25 Hz. In experiment II, cylinder #1 and cylinder #2 are of the same type. The reversing frequency of directional control valves #1 and #2 is 0.50 Hz.

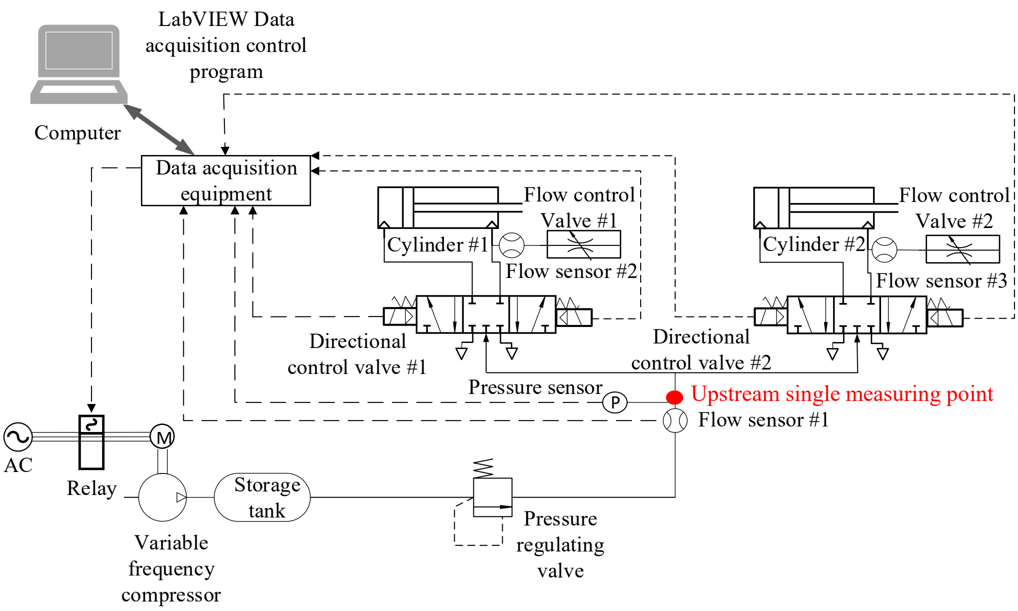

Figure 1. Schematic diagram of the experimental system.

Table 1. Main components and parameters of experimental system.

Components	Manufacturer	Model Number	Main Parameters
Variable frequency compressor	Fusheng Industrial (Shanghai, China)	SA+06A-8F	0.78 m^3/min, 9.8 kW/(m^3/min), 0.85 MPa
Flow sensor	FESTO (Jinan, China) SMC (Beijing, China)	SFAB-600U-HQ10-2SV-M12 PF2M750S-01-EW-M	6~600 L/min, 0~10 MPa 0.5~50 L/min, 0~0.75 MPa
Pressure sensor	SMC (Beijing, China)	ISE40A-C6-R-M	−0.1~1.0 MPa
Three-position five-way directional valve	SMC (Beijing, China)	SY5320-5LZD-01	0.2~0.7 MPa
Pressure-regulating valve	SMC (Beijing, China)	IVT1050-211L	0.005~0.9 MPa
Cylinder	SMC (Beijing, China)	MDBB32-200Z MDBB32-400Z	Φ32 mm, 200 mm Φ32 mm, 400 mm
Computer	Advantech (Taiwan, China)	IPC-610L	I5-4200, 4 g, 1 t
Data acquisition equipment	Advantech (Taiwan, China)	PCI-1710U PCI-10168-2E PCLD-8710 PCL-10120-2E	16 AI, 12 bit, 2 AO, 12 bit, 16 DI, 5 V/TTL, 16 DO, 5 V/TTL:100 kS/s

Table 2. Two sets of experiments.

Experiment	Cylinder #1	Cylinder #2	The Reversing Frequency of Solenoid Reversing Valves #1 and #2
Experiment I	Type A cylinder	Type B cylinder	0.25 Hz
Experiment II	Type A cylinder	Type A cylinder (delay)	0.50 Hz

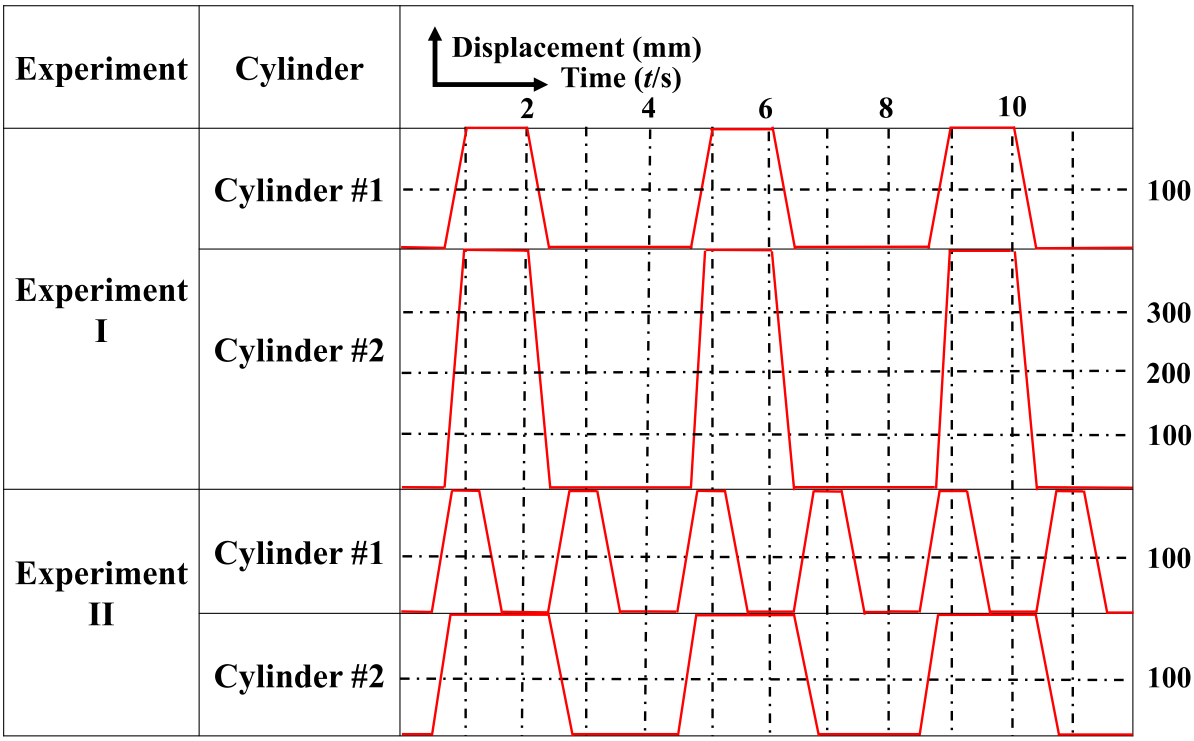

Figure 2. Work paces of two cylinders in experiment I and experiment II.

Flow sensor #2 and flow sensor #3 measure the leakage range of cylinder #1 and cylinder #2, respectively. Pressure sensor and flow sensor #1 collect the pressure and flow data of the single measurement point upstream of the pneumatic circuit. The data can be collected and controlled directly by the computer. The sampling frequency is set to 100 Hz. In experiment I and experiment II, a complete signal cycle is defined as four seconds, that is, 400 data points in a cycle. The pressure-regulating valve is used to adjust the pressure downstream. In this study, the setting pressure of the pressure-regulating valve is set to 0.35 MPa.

2.2. Exergy of Compressed Air

The pressure signal and flow rate signal are the most widely used factors for diagnosing leakage faults in pneumatic systems. However, due to the significant compressibility of gas, pressure and flow rate are coupled and intertwined. Pneumatic power transmission involves transmitting energy through compressed gas, and different transmission processes exhibit different energy consumption patterns. Thus, understanding the energy consumption characteristics is essential for clarifying transmission characteristics and further diagnosing different faults. In recent years, exergy analysis based on the second law of thermodynamics has been widely studied and found to be suitable for quantitatively evaluating the energy of compressed air in pneumatic systems [28]. Additionally, from the perspective of data fusion, the exergy of compressed air can be regarded as a fusion of pressure, flow rate, and temperature. Compared with single pressure signals or single flow rate signals, fusion information of exergy is predicted to be more accurate and reasonable for monitoring states of pneumatic components and improving the accuracy of pattern recognition and fault diagnosis. Thus, in this study, pressure data, flow rate data, and exergy data are all investigated and compared to reveal which is the best.

In industrial pneumatic systems, there is usually no chemical reaction, and the changes in kinetic energy and potential energy of compressed air generally can be ignored. The pressure of compressed air is generally below 1 MPa, so compressed air can be regarded as an ideal gas. In the pneumatic system discussed in this study, the temperature fluctuations in the environment and the system are negligible. Therefore, the exergy of compressed air can be simplified and calculated by the following equation

$$\dot{E}_x = \dot{m}e_x = \dot{m}T_0R_g\ln\frac{p}{p_0}, \tag{1}$$

where $\dot{E}_x$ is the total exergy flow rate (kJ/s), $\dot{m}$ is the mass flow rate of compressed air (kg/s), e_x is the specific exergy (kJ/kg), T is the temperature (K), R_g is the gas constant (kJ/(kg·K)), p is the pressure (Pa), and the subscript 0 represents the reference state. Exergy denotes the maximum useful work that can be obtained when the system and the environment are balanced. Therefore, it is very important to clearly define the reference environment. In this study, the reference pressure is set to 101,325 Pa.

2.3. Experiment Settings

Two sets of experiments, experiment I and experiment II, are conducted to simulate different working conditions. In experiment I and experiment II, nine operating states of parallel-installed cylinders are simulated. One is the normal working state without any faults and the other eight states are abnormal working states with different levels of leakage faults. For each working state, the number of training set samples is 200, the number of validation set samples is 10, and the number of test set samples is 20. Each sample contains 400 continuous sampling points. The fault types and characteristics of experiment I are shown in Table 3, and the dataset information is shown in Table 4. The fault types and characteristics of experiment II are shown in Table 5, and the dataset information is shown in Table 6. The simulated leakage refers to the external leakage at the rod side of the cylinder.

Table 3. Types and characteristics of faults in experiment I.

Fault Type	Fault Level of Cylinder #1 (L/min)	Fault Level of Cylinder #2 (L/min)
Normal	0	0
Fault #1	5	0
Fault #2	0	5
Fault #3	15	0
Fault #4	0	15
Fault #5	25	0
Fault #6	0	25
Fault #7	35	0
Fault #8	0	35

Table 4. Dataset information of experiment I.

Fault Type	Number of Samples in the Training Set	Number of Samples in the Verification Set	Number of Samples in the Test Set
Normal	200	10	20
Fault #1	200	10	20
Fault #2	200	10	20
Fault #3	200	10	20
Fault #4	200	10	20
Fault #5	200	10	20
Fault #6	200	10	20
Fault #7	200	10	20
Fault #8	200	10	20

Table 5. Types and characteristics of faults in experiment II.

Fault Type	Fault Level of Cylinder 1 (L/min)	Fault Level of Cylinder 2 (L/min)
Normal	0	0
Fault #1	5	0
Fault #2	0	5
Fault #3	15	0
Fault #4	0	15
Fault #5	25	0
Fault #6	0	25
Fault #7	35	0
Fault #8	0	35

Table 6. Dataset information of experiment II.

Fault Type	Number of Samples in the Training Set	Number of Samples in the Verification Set	Number of Samples in the Test Set
Normal	200	10	20
Fault #1	200	10	20
Fault #2	200	10	20
Fault #3	200	10	20
Fault #4	200	10	20
Fault #5	200	10	20
Fault #6	200	10	20
Fault #7	200	10	20
Fault #8	200	10	20

3. Methodology

3.1. Data Preparation

Figure 3a,c,e show the intercepted original signals of upstream flow rate, pressure, and exergy acquired in experiment I. Figure 3b,d,f display the intercepted original signals in experiment II. These signals present obvious periodicities which are related to the reversing frequency of the directional control valve.

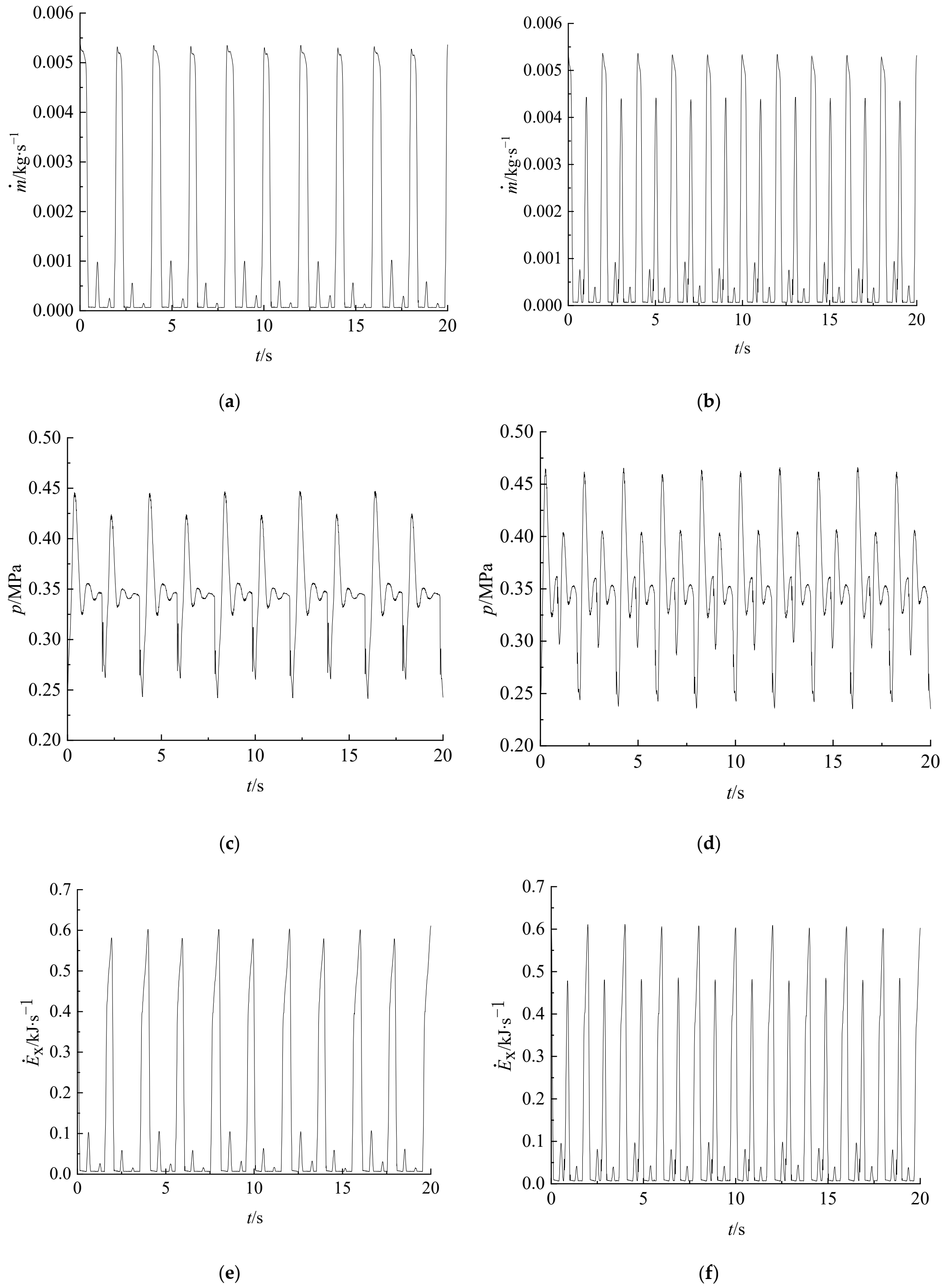

Figure 3. Original signals of upstream flow rate, pressure, and exergy in experiments I and II. (**a**) Single-cycle raw flow data in experiment I. (**b**) Single-cycle raw flow data in experiment II. (**c**) Single-cycle raw pressure data in experiment I. (**d**) Single-cycle raw pressure data in experiment II. (**e**) Single-cycle raw exergy data in experiment I. (**f**) Single-cycle raw exergy data in experiment II.

The noise, missing values, repeated values, and outliers in the originally collected data challenge the performance of machine learning models. Therefore, data preprocessing is necessary for the following data analysis and fault diagnosis. High-quality data could generally lead to higher diagnostic accuracy. Proper preprocessing of the original features is necessary to apply SAE models and machine learning classification models such as GPC, SVM, and KNN more effectively in this study. Through data preprocessing, it makes the learning and processing of the algorithm easier. This improves the accuracy and efficiency of the subsequent feature extraction process. The data preprocessing process used in this study is shown in Figure 4.

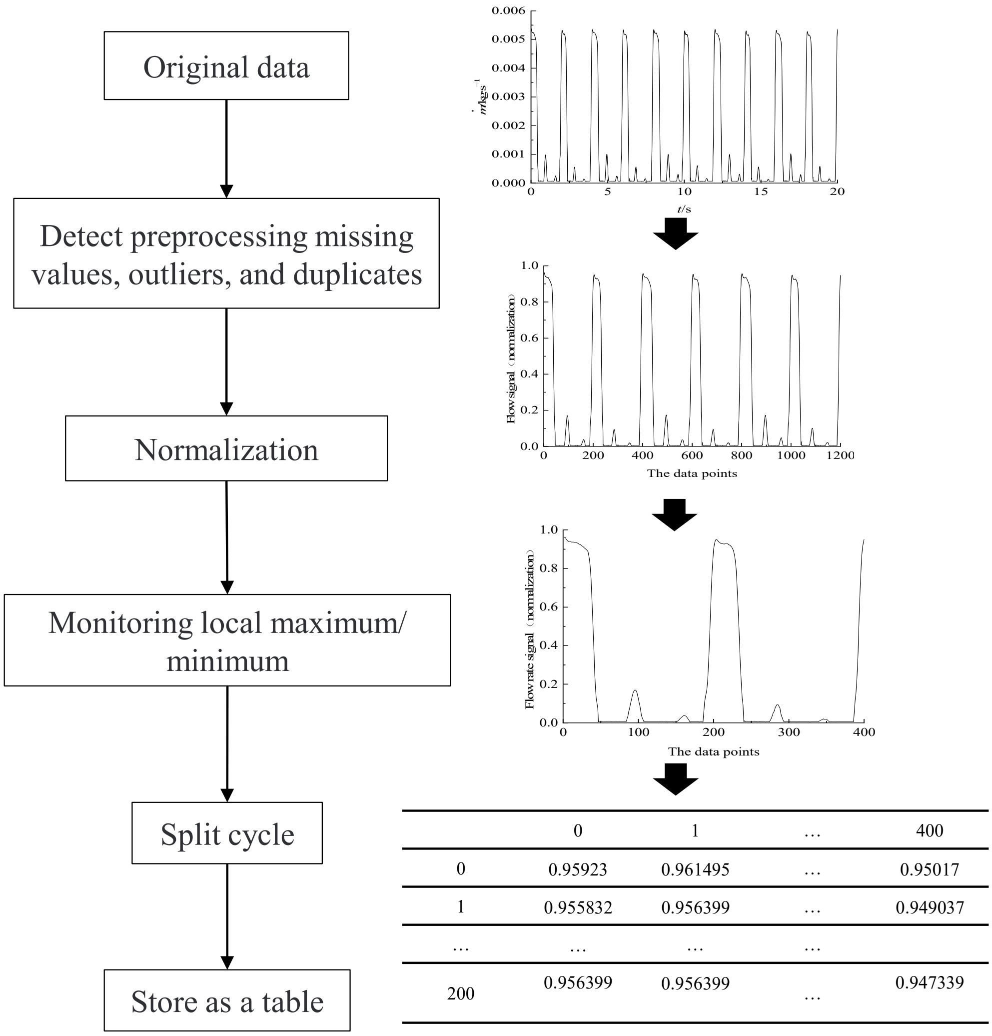

	0	1	…	400
0	0.95923	0.961495	…	0.95017
1	0.955832	0.956399	…	0.949037
…	…	…	…	
200	0.956399	0.956399	…	0.947339

Figure 4. Flow chart of the original data preprocessing.

Firstly, low-correlation information such as missing values, outliers, and repeated values are detected and eliminated from the collected original signals, thereby outputting high-quality and reliable data. To ensure comparability of characteristics across different dimensions, each sample is normalized using unit norm scaling in Python. Through data normalization, the data can be projected onto the [0,1] interval without changing the distribution of the original data. Normalizing the dataset is more conducive to machine learning algorithms. Figure 5a,c,e show a single cycle of the upstream flow, pressure, and exergy of experiment I, and Figure 5b,d,f show a single cycle of the upstream flow, pressure, and exergy of experiment II.

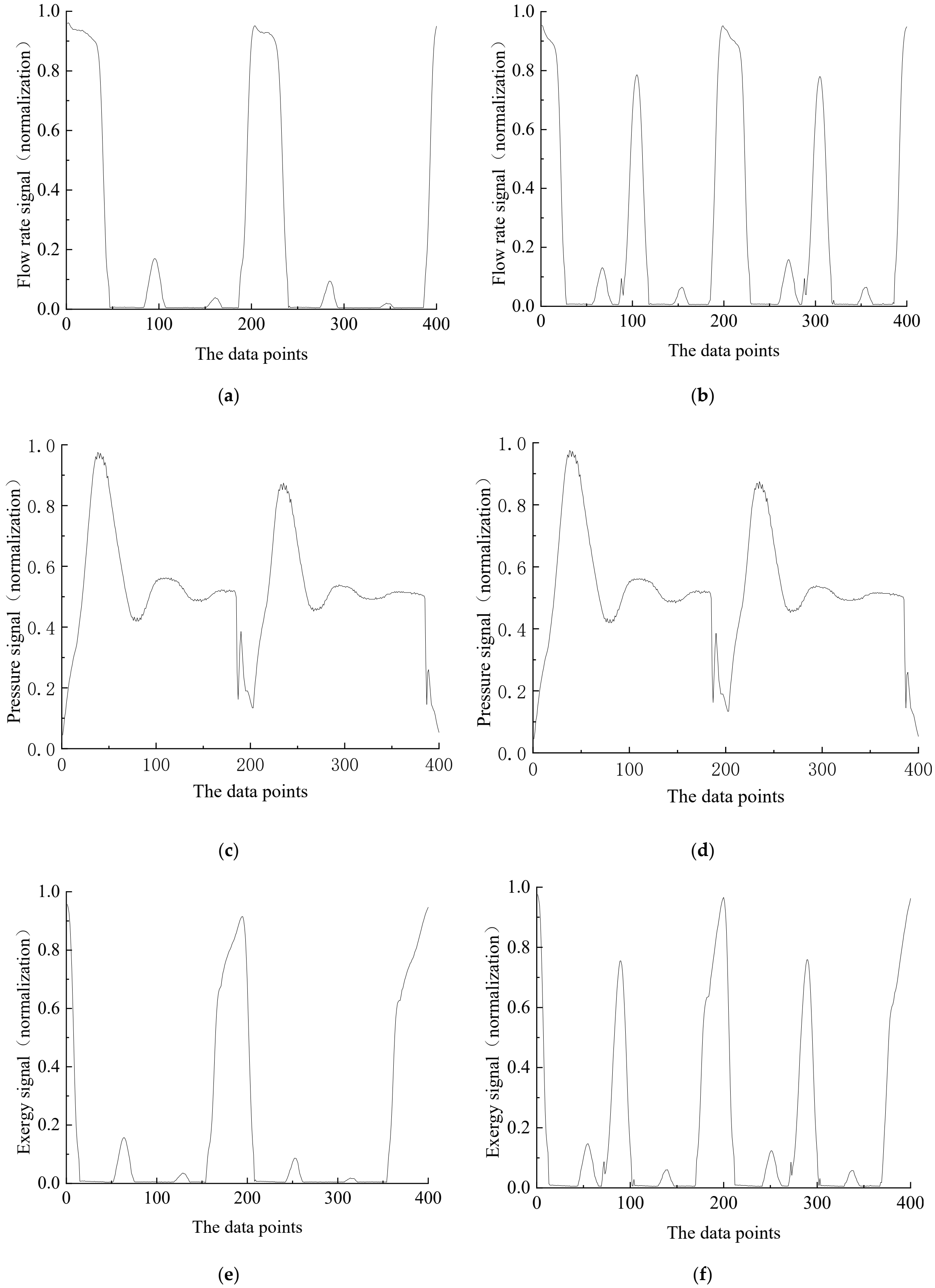

Figure 5. A single cycle of upstream flow rate, pressure, and exergy in experiments I and II. (**a**) A single cycle of flow rate data in experiment I. (**b**) A single cycle of flow rate data in experiment II. (**c**) A single cycle of pressure data in experiment I. (**d**) A single cycle of pressure data in experiment II. (**e**) A single cycle of exergy data in experiment I. (**f**) A single cycle of exergy data in experiment II.

Cycle segmentation is a critical step in preprocessing. As the signal is regular and periodic, each cycle is selected as a sample for the machine learning process. Each starting point is identified using Python, and the signal is segmented by setting a moving window. The segmented signal is then stored in a table for further processing.

3.2. Stacked Auto-Encoders

An auto-encoder (AE) is initially applied as a structurally symmetric neural network in the image data processing. Its function is to compress input images or signals into an inexpressible state and then reconstruct the images through an inverse process. Therefore, AE is commonly used for the dimensionality reduction of high-dimensional signals, compressing input signals into very small dimensions without losing important information from the original signals. The basic structure of an AE, as shown in Figure 6, consists of an input layer, a hidden layer, and an output layer. The input layer represents the input data, the output layer reconstructs the input data, and the hidden layer represents the most representative features extracted by the AE. With these features, an AE can reconstruct the original signals and output them via the output layer. The process of feature extraction is referred to as encoding, while the reconstruction process is referred to as decoding. Therefore, when using an AE as a tool for feature extraction, the effectiveness of the encoder in extracting features can be demonstrated by comparing the reconstructed signals with the original signals [29].

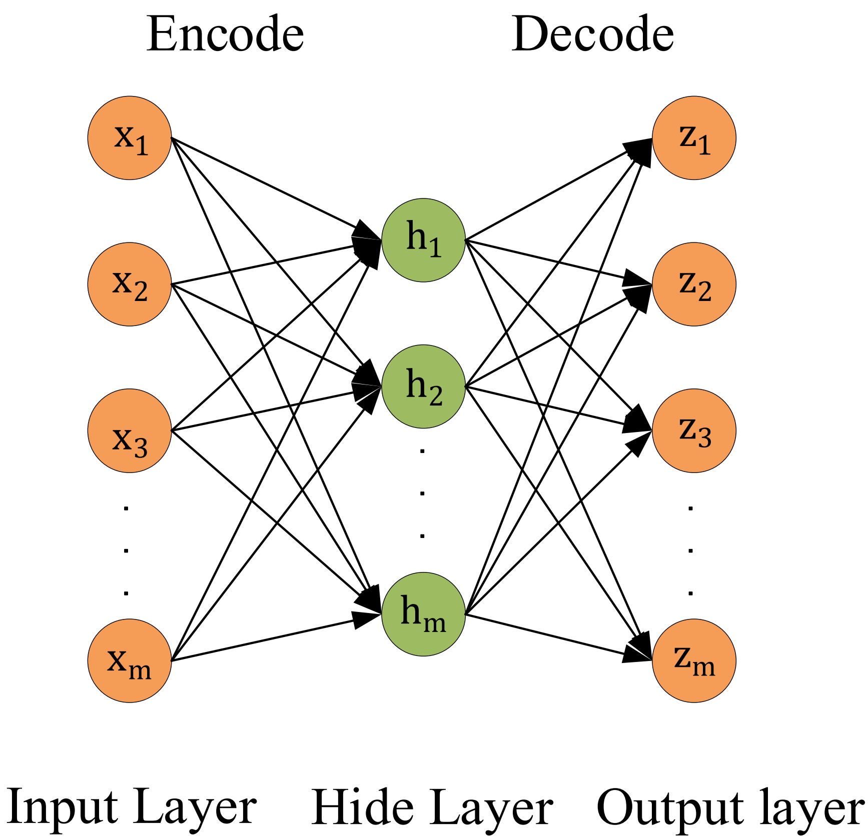

Figure 6. Structure of Auto-Encoder.

Suppose the input vector sample set is $x = (x_1, x_2, \cdots, x_i, \cdots, x_m)$. The encoder network and the decoding network can be expressed as

$$\mathrm{h} = s(\mathrm{Wx} + \mathrm{b}), \tag{2}$$

$$z = s\left(\mathrm{W}'\mathrm{h} + \mathrm{b}'\right), \tag{3}$$

where h is the hidden layer feature, z is the approximate recovery data of the original input, s is the activation function, W and W′ are the weight matrix of the coding network and decoding network, respectively, and b and b′ are the bias vectors of the encoding network and the decoding network, respectively.

The loss function of an AE is commonly defined by mean square error (MSE) as follows

$$L = \frac{1}{k}\|x_i - z_i\|^2, \tag{4}$$

where k is the dimension of the input vector, and $\|.\|$ represents the norm.

Therefore, the total loss function of m samples is

$$J = \frac{1}{m}\sum_{i=1}^{m} L(x, z). \tag{5}$$

A SAE is a series of autoencoders connected step by step [30]. Figure 7 is the structure diagram of SAE.

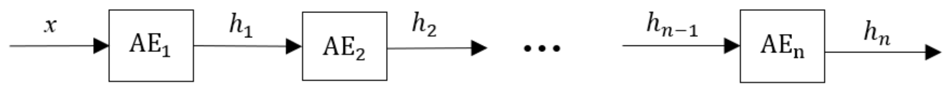

Figure 7. Structure of SAE.

The training process of SAE is shown as follows. Firstly, $\boldsymbol{x}$ is used as the input data of the first auto-encoder AE_1, and the network parameters $\{W_1, b_1\}$ and the low-dimensional feature h_1 of the hidden layer are obtained by training. Then, h_1 is used as the input data of the second auto-encoder AE_2, and the network parameters $\{W_2, b_2\}$ and its low-dimensional feature h_2 of AE_2 are obtained by training. This continues until the network parameter $\{W_m, b_m\}$ and the low-dimensional feature h_m of the last auto-encoding AE_m are finally obtained.

3.3. Diagnostic Process

The flow chart for diagnosing the leakage faults in this study is presented in Figure 8. The detailed steps are explained as follows.

1. The original flow rate, pressure, and exergy data are collected and preprocessed twice at the upstream single measurement point. The data collected for the first time are divided into a training set and a verification set, while the data collected for the second time are treated as the test set.
2. A SAE model is built in Python, and fundamental parameters, such as the number of hidden layers, iterative parameters, and activation functions, are set.
3. The training set undergoes dimensionality reduction and feature extraction via SAE. The parameters, including the number of iterations and the choice of activation function, are adjusted based on the classification results obtained from the validation set [31–33].
4. The machine learning classification model (GPC, SVM, KNN) is trained using the training set. Through the validation set results, the parameters of the machine learning classification models are adjusted to be optimal.
5. The test set is analyzed by the trained SAE model and machine learning classification models for fault diagnosis. The accuracy, macro-precision, macro-recall, and macro-F1-score of the test set are evaluated. The training time, prediction time, and storage space of different classifiers are recorded for comparison.

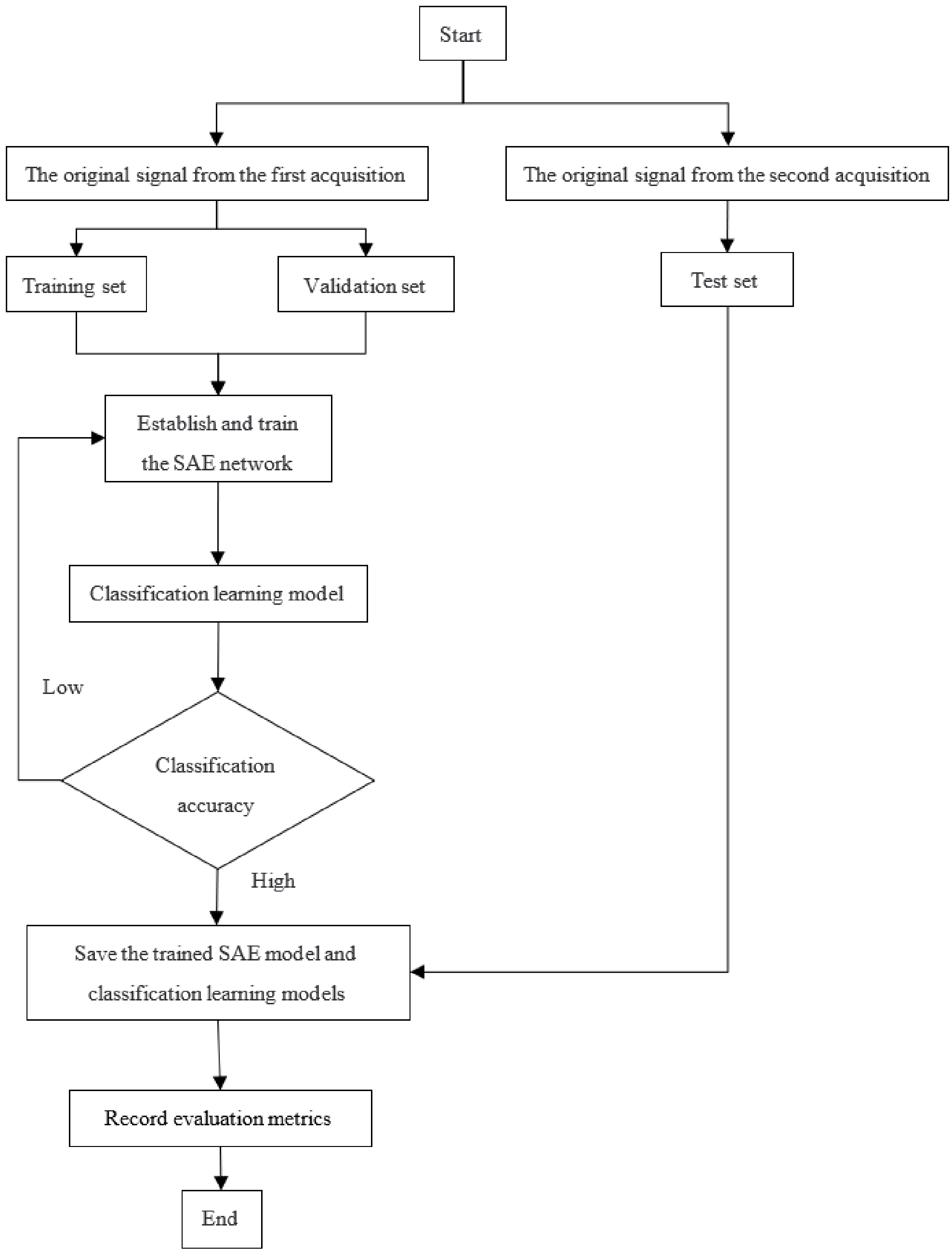

Figure 8. Flow chart of diagnosis.

3.4. Evaluation Metrics

To compare the performance of the three classifiers (GPC, SVM, and KNN) used in this study, several evaluation metrics are selected. This study focuses on multi-classification problems with equal test samples for each class; there is no imbalance issue. Thus, accuracy can be used as one of the main indicators. It is easy to utilize and can directly reflect the overall prediction accuracy of a classifier. Macro-precision, macro-recall, and macro-F1-score are also introduced for a comprehensive assessment of a classifier's overall performance. Moreover, the training time, prediction time, and storage space of classifiers are considered the computational complexity indicators for evaluating the practical application efficiency of classifiers. The definitions and principles of these metrics are explained as follows.

Accuracy: Accuracy is the ratio of correctly predicted samples to total samples. It measures the classification accuracy of the classifier on the entire dataset. Accuracy is one of the most commonly used evaluation metrics. However, accuracy may be affected by an imbalanced dataset.

Precision: Precision is the ratio of true positive samples to those predicted as positive by the classifier. It measures the accuracy of the classifier in predicting positive samples. The formula for calculating precision is as follows: precision = (number of true positive samples)/(number of samples predicted as positive).

Recall: Recall is the ratio of true positive samples to actual positive samples. It measures the coverage of the classifier for actual positive samples. The formula for calculating the recall is as follows: recall = (number of true positive samples)/(number of actual positive samples).

F1-Score: F1-score is the harmonic mean of precision and recall, considering both the accuracy and coverage of the classifier. The formula for F1-score is as follows: F1-score = 2 × (precision × recall)/(precision + recall).

Macro-precision: Macro-precision measures the average precision of the classifier for each class, macro-recall measures the average coverage of the classifier for each class, and macro-F1-score considers the balance between precision and recall.

Training Time: Training time refers to the time required to train the classifier. It represents the time the classifier needs to learn the model on a given dataset. Training time is an important metric, especially for large-scale datasets and complex classification algorithms. A shorter training time means the classifier can learn the model and make predictions more quickly.

Prediction Time: Prediction time refers to the time required to make classifications and predictions on new samples. Prediction time is a critical metric, particularly in real-time applications where fast prediction speed is essential.

Storage Space: Storage space refers to the space required to store the trained classifier model. It represents the space occupied by the classifier in memory. Storage space is an important consideration for limited computational resources.

Overall, with these metrics, it is possible to comprehensively evaluate the performance of the GPC, SVM, and KNN classifiers used in this study. This evaluation provides clear recommendations for future applications.

4. Results and Discussion

4.1. Analysis of SAE Feature Extraction Results

Effective feature extraction and dimensionality reduction can achieve a compact representation of data, reduce noise, and further improve the efficiency of learning and classification. Because the pressure, flow rate, and exergy data of samples are high-dimensional, the SAE is used for extracting features and reducing dimensions. Thus, it is important to evaluate the effectiveness of feature extraction.

In this study, the activation functions of Relu and Sigmoid are used. The SAE network structure is set as [400, 200, 100, 50, 10]. The number of hidden layers is set to four, and the number of iterations is set to 300. As the SAE belongs to the neural network, the loss curves of the training dataset and the verification dataset are visually analyzed to evaluate whether there is overfitting. Figure 9a,c,e show the loss curves of the training dataset and the validation dataset of flow rate, pressure, and exergy, respectively, in experiment I. Figure 9b,d,f show the loss curves of the training dataset and the validation dataset of flow rate, pressure, and exergy, respectively, in experiment II. When the visualization of the loss function gradually approaches zero, this means that the value of the loss function gradually decreases, which indicates that the quality of feature extraction is improving. On the contrary, if the visualization results show obvious fluctuations, it means that the value of the loss function has a large change, which may imply that the results of feature extraction are not stable and not good enough.

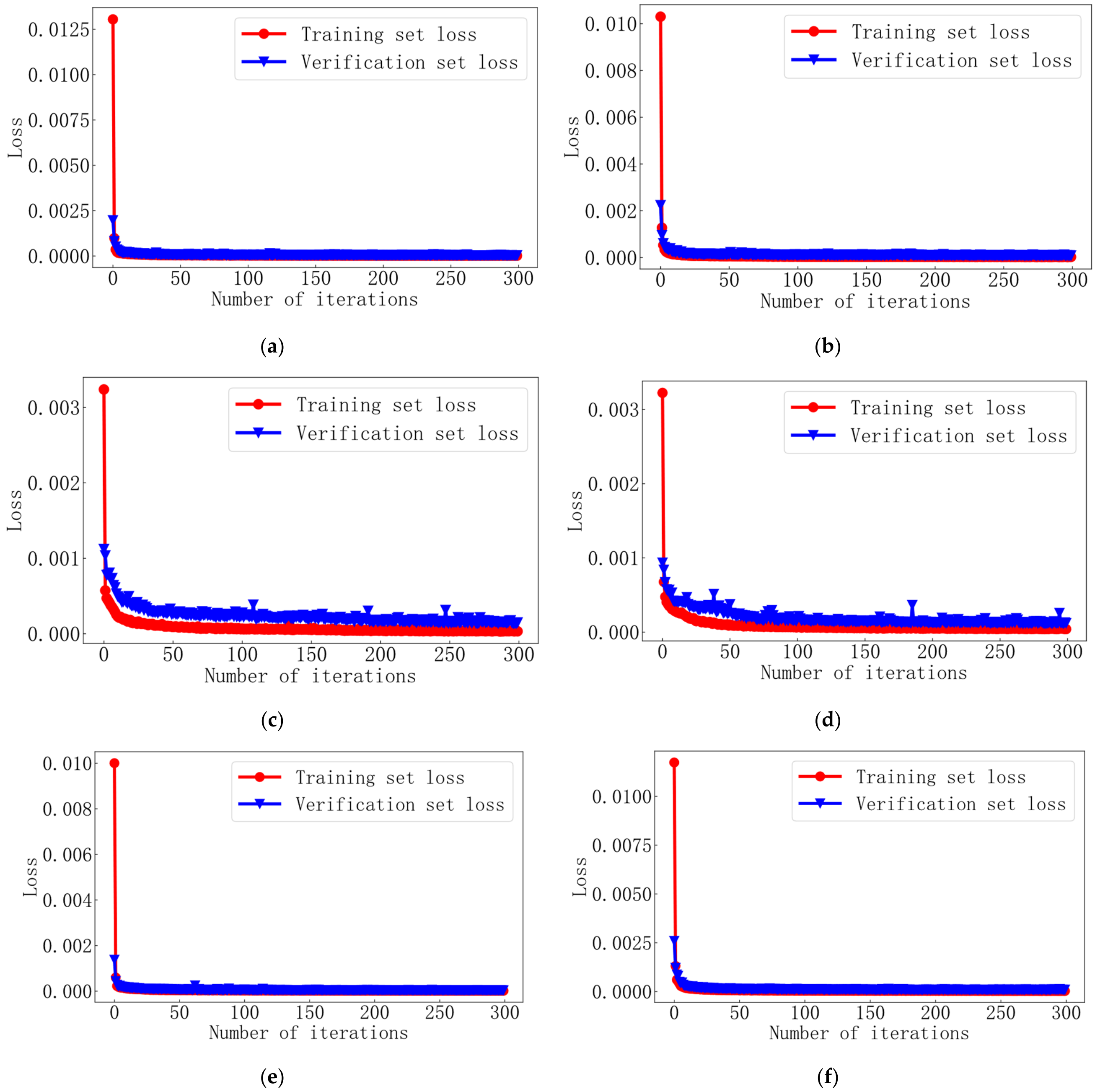

Figure 9. SAE loss curves for experiments I and II. (**a**) Loss curves of training dataset and validation dataset of flow rate in experiment I. (**b**) Loss curves of training dataset and validation dataset of flow rate in experiment II. (**c**) Loss curves of training dataset and validation dataset of pressure in experiment I. (**d**) Loss curves of training dataset and validation dataset of pressure in experiment II. (**e**) Loss curves of training dataset and validation dataset of exergy in experiment I. (**f**) Loss curves of training dataset and validation dataset of exergy in experiment II.

Figure 10 presents the input original profiles and output reconstructed profiles of the flow rate, pressure, and exergy signals in experiment I. Figure 11 shows those in experiment II. It can be seen that the data after dimension reduction via SAE restore the dominating characteristics of the input data well. This also means that the trained SAE model can effectively reduce the dimension and reconstruct the original data. It can be seen from the red circle that when the input data are accurately reconstructed, the dimensionality reduction data of the hidden layer of the SAE contain enough information to express the key features of the original data. This means that the low-dimensional representation learned by the encoder can retain important information in the original data and can reconstruct a high-quality output during the decoding process.

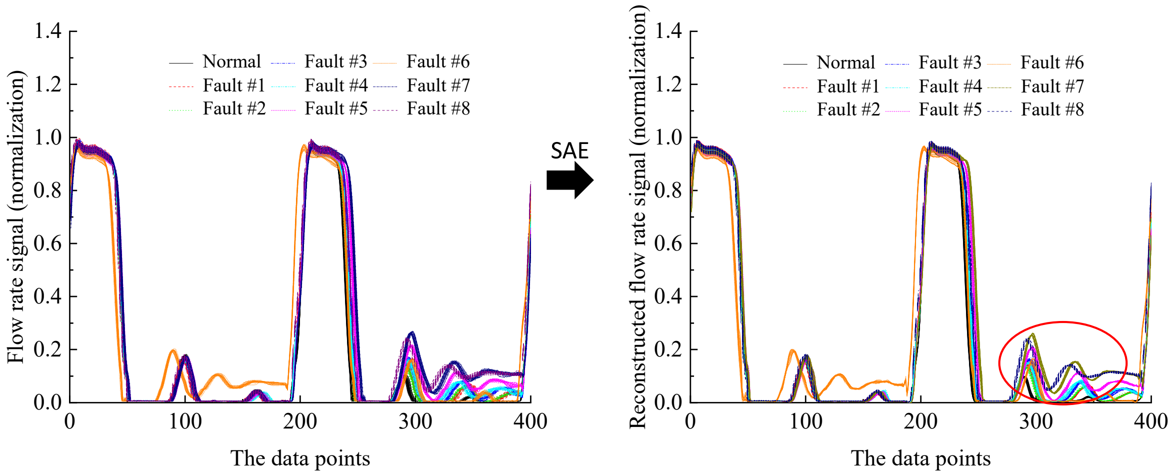

(**a**)

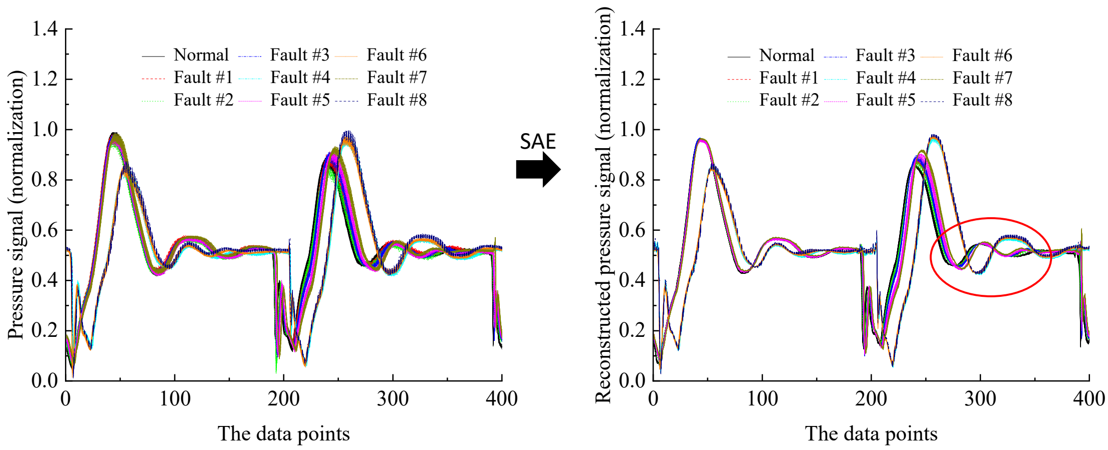

(**b**)

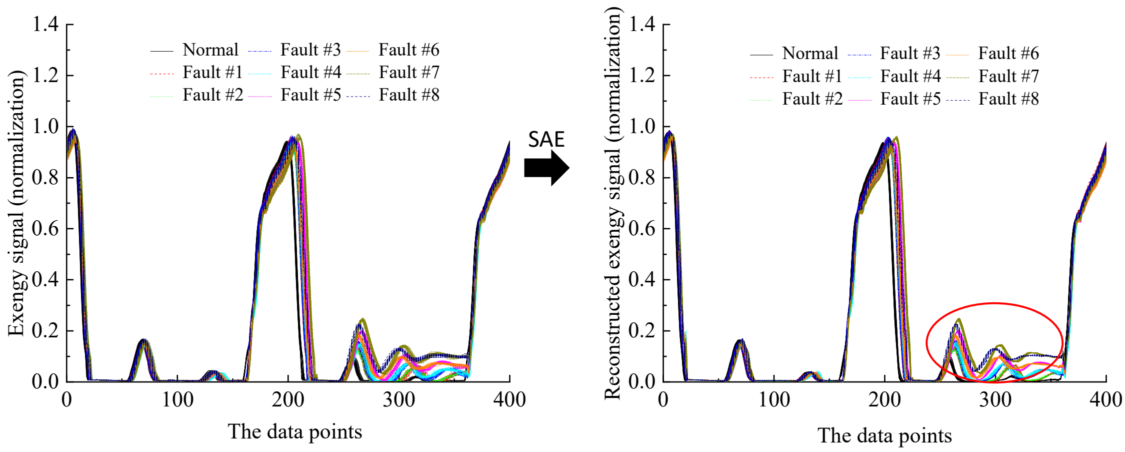

(**c**)

Figure 10. Comparison of original and reconstructed flow rate, pressure, and exergy signals for experiment I using SAE. (**a**) Comparison of original and reconstructed flow rate signals for experiment I. (**b**) Comparison of original and reconstructed pressure signals for experiment I. (**c**) Comparison of original and reconstructed exergy signals for experiment I.

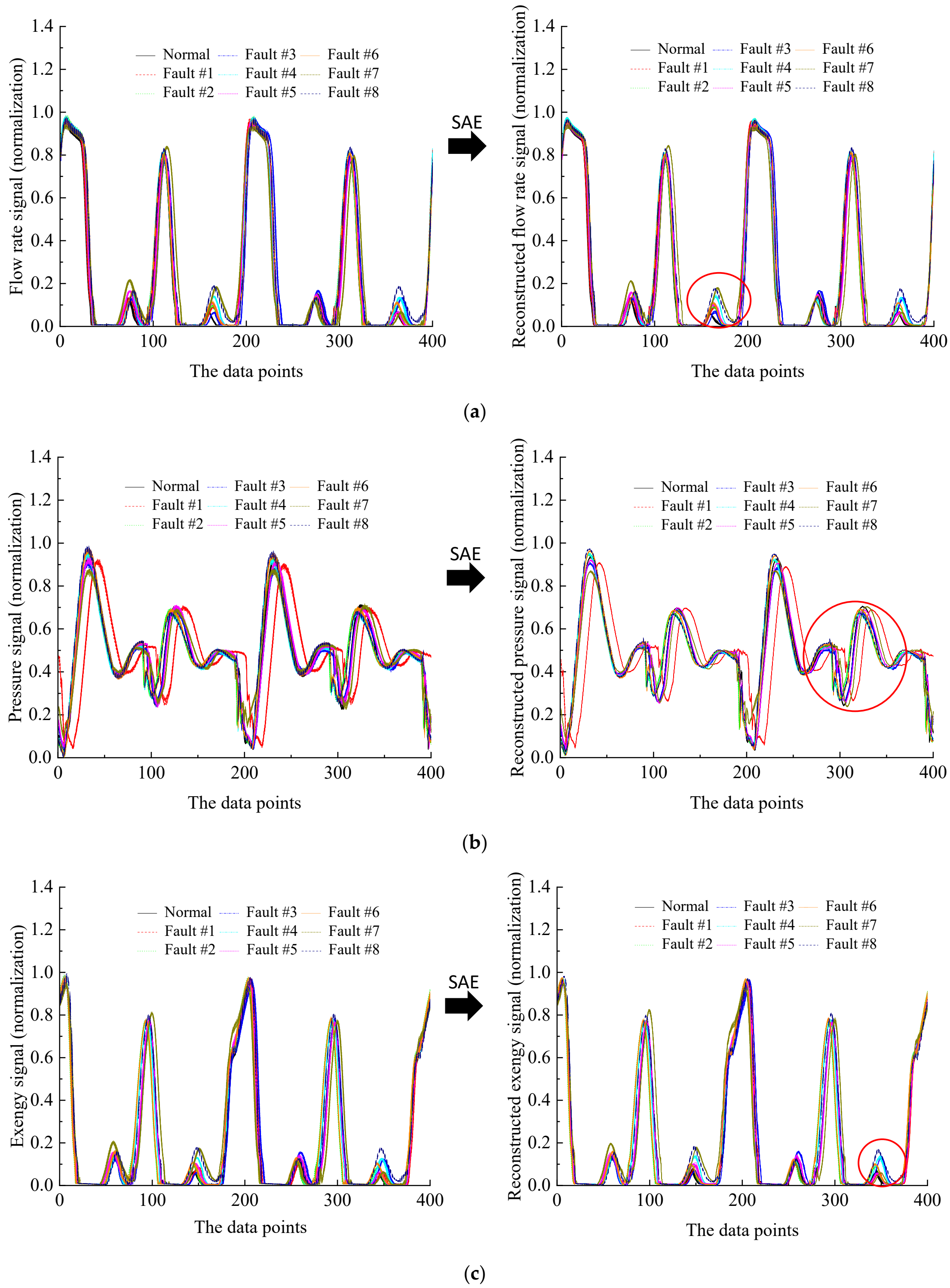

Figure 11. Comparison of original and reconstructed flow rate, pressure, and exergy signals for experiment II using SAE. (**a**) Comparison of original and reconstructed flow rate signals for experiment II. (**b**) Comparison of original and reconstructed pressure signals for experiment II. (**c**) Comparison of original and reconstructed exergy signals for experiment II.

4.2. Comparison of Different Signals

The extracted features via SAE are sent to the machine learning model (GPC, SVM, and KNN in this study) for learning and classification. The code for the three classifiers is implemented using Python's built-in function libraries.

In the GPC model, the covariance function is equivalent to the kernel function. Firstly, the initial mean, likelihood, and covariance functions are used to train the data, and convergence is achieved after 200 iterations. The mean, likelihood, and covariance functions are automatically updated, and all hyperparameters are obtained. After determining the hyperparameters, the leakage fault feature vector of the test set is input into the GPC model to output the probability of each fault, and the fault state corresponding to the maximum probability is taken as the diagnosis result.

The kernel function of SVM adopts the RBF kernel function, and the penalty factor and kernel function parameters are set to 10 and 0.1, respectively. The KNN model uses the number of neighbors for the neighbor's query by default, and the number of neighbors is three in this study.

Table 7 shows the accuracies of ten tests of three machine learning algorithms in experiment I. In experiment I, when the GPC algorithm is used, the average accuracy of the flow rate signal, pressure signal, and exergy signal is 98.99%, 77.38%, and 100%, respectively. When the SVM algorithm is used, the average accuracy of the flow rate signal, pressure signal, and exergy signal is 98.38%, 85.95%, and 100%, respectively. For KNN, the average accuracy of the flow rate signal, pressure signal, and exergy signal is 98.21%, 66.71%, and 99.83%, respectively. Table 8 shows the corresponding results in experiment II. In experiment II, for GPC, the average accuracy of the flow rate signal, pressure signal, and exergy signal is 98.05%, 89.55%, and 99.94%, respectively. For SVM, the corresponding values could reach 95.15%, 93.50%, and 100%, respectively. For KNN, the corresponding values are 91.67%, 87.39%, and 92.50%, respectively. Thus, the results indicate that it is possible to diagnose leakage faults of two parallel-installed pneumatic cylinders with data collected from a single upstream point. This can be easily expanded to a more complex system with more parallel-installed pneumatic cylinders.

Table 7. Accuracy of experiment I for ten tests.

Classifiers	Signal	Test Result										Average Accuracy
		1	2	3	4	5	6	7	8	9	10	
GPC	Flow rate	97.22%	98.88%	100%	100%	100%	98.88%	98.88%	100%	98.33%	97.77%	98.99%
	Pressure	76.66%	88.33%	76.66%	76.11%	76.66%	83.33%	76.66%	77.77%	67.22%	74.44%	77.38%
	Exergy	100%	100%	100%	100%	100%	100%	100%	100%	100%	100%	100%
SVM	Flow rate	98.33%	98.88%	100%	100%	100%	100%	99.44%	100%	100%	97.22%	99.38%
	Pressure	87.77%	88.88%	86.66%	79.44%	87.77%	86.66%	93.33%	85.55%	85.00%	78.44%	85.95%
	Exergy	100%	100%	100%	100%	100%	100%	100%	100%	100%	100%	100%
KNN	Flow rate	96.11%	97.77%	100%	100%	98.33%	96.66%	97.77%	98.33%	99.44%	97.77%	98.21%
	Pressure	72.22%	71.11%	71.66%	66.66%	75.00%	70.00%	75.55%	72.77%	68.88%	67.77%	66.71%
	Exergy	100%	100%	100%	100%	98.33%	100%	100%	100%	100%	100%	99.83%

Table 8. Accuracy of experiment II for ten tests.

Classifiers	Signal	Test Result										Average Accuracy
		1	2	3	4	5	6	7	8	9	10	
GPC	Flow rate	100%	98.88%	99.44%	99.44%	97.77%	90.55%	100%	100%	97.22%	97.22%	98.05%
	Pressure	92.77%	82.77%	89.44%	88.88%	88.88%	92.77%	90.00%	90.00%	88.33%	91.66%	89.55%
	Exergy	100%	100%	100%	100%	99.44%	100%	100%	100%	100%	100%	99.94%
SVM	Flow rate	97.77%	96.66%	93.88%	91.66%	97.72%	90.55%	97.77%	94.44%	94.44%	96.66%	95.15%
	Pressure	97.77%	85.55%	96.11%	96.11%	90.55%	94.44%	93.88%	93.33%	88.33%	98.88%	93.50%
	Exergy	100%	100%	100%	100%	100%	100%	100%	100	100%	100%	100%
KNN	Flow rate	92.22%	99.55%	89.44%	88.88%	91.11%	88.88%	90.55%	93.33%	89.44%	93.33%	91.67%
	Pressure	84.44%	85.55%	88.33%	88.37%	88.33%	90.00%	88.37%	88.33%	83.33%	88.88%	87.39%
	Exergy	90.05%	97.22%	94.44%	96.11%	93.88%	92.77%	92.22%	88.33	90.00%	90.00%	92.50%

Figures 12 and 13 depict the average accuracy of fault diagnosis for the flow rate, pressure, and exergy signals with different algorithms in experiments I and II, respectively. It is more intuitively visible from the figures that the average accuracy based on the exergy signal is higher than that based on the flow rate signal and significantly higher than that based on the pressure signal.

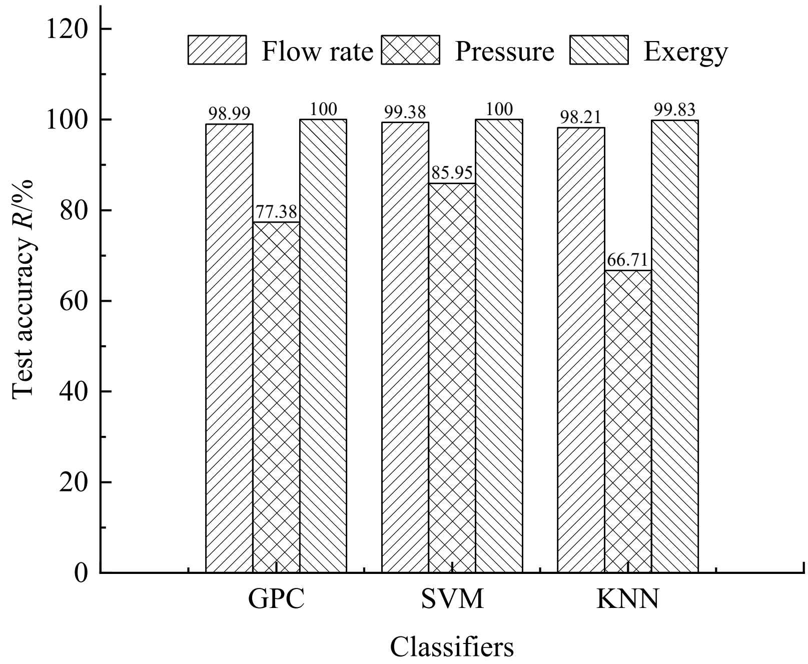

Figure 12. The average accuracy of GPC, SVM, and KNN classifiers in experiment I.

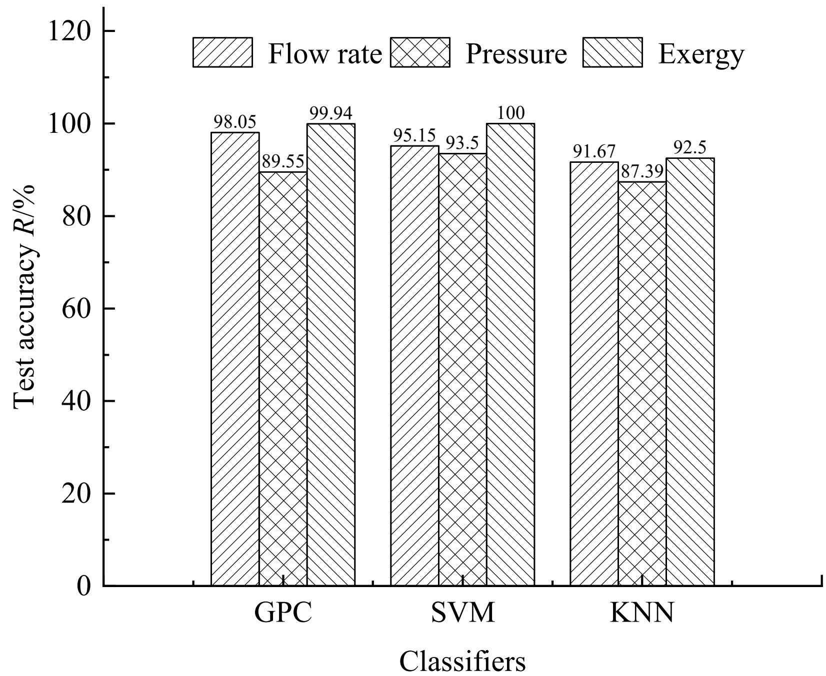

Figure 13. The average accuracy of GPC, SVM, and KNN classifiers in experiment II.

In experiment I, three different classifiers are used to test the flow, pressure, and signal. The results indicate that the average accuracy of the three classifiers based on the flow signal is 98.86%, the average accuracy of the three classifiers based on the pressure signal is 76.68%, and the average accuracy of the three classifiers based on the exergy signal is

99.94%. Therefore, it can be observed that the exergy signal performs best, followed by the flow rate signal and the pressure signal. Similarly, in experiment II, the results reveal that the average accuracy of the three classifiers based on the flow rate signal is 94.95%, the average accuracy of the three classifiers based on the pressure signal is 90.14%, and the average accuracy of the three classifiers based on the exergy signal is 97.48%. It is noticeable that the exergy signal still performs the best. The average accuracy based on the pressure signal increases evidently. Thus, these results signify that the exergy signal performs better than the flow rate and pressure signals under different working conditions investigated in this study. That is, the accuracy based on the exergy signal is the least sensitive to the working conditions and machine learning algorithms.

Tables 9 and 10 show the macro-precision, macro-recall, and macro-F1-score of different machine learning algorithms for different signals in experiment I and experiment II, respectively. The values in the table are the average values of the three tests.

Table 9. Comparison of macro-precision, macro-recall, and macro-F1-score for different signals in experiment I.

Classifiers	Signal	Macro-Precision	Macro-Recall	Macro-F1-Score
GPC	Flow rate	1	1	1
	Pressure	0.847	0.83	0.81
	Exergy	1	1	1
SVM	Flow rate	1	1	1
	Pressure	0.96	0.96	0.95
	Exergy	1	1	1
KNN	Flow rate	0.99	0.99	0.99
	Pressure	0.79	0.76	0.74
	Exergy	1	1	1

Table 10. Comparison of macro-precision, macro-recall, and macro-F1-score for different signals in experiment II.

Classifiers	Signal	Macro-Precision	Macro-Recall	Macro-F1-Score
GPC	Flow rate	0.99	0.99	0.99
	Pressure	0.94	0.90	0.87
	Exergy	0.99	0.99	0.99
SVM	Flow rate	0.99	0.99	0.99
	Pressure	0.95	0.91	0.89
	Exergy	1	1	1
KNN	Flow rate	0.98	0.98	0.98
	Pressure	0.81	0.86	0.82
	Exergy	0.99	0.99	0.99

In both experiment I and experiment II, the macro-precision, macro-recall, and macro-F1-score for the flow rate signal and exergy signal are nearly 1 for all algorithms, thereby indicating high performance. However, the macro-precision, macro-recall, and macro-F1-score for the pressure signal are lower, which means poorer classification performance compared to the other signals. In terms of leakage faults, the pressure signal may provide limited or less distinct feature information. If the patterns or variations related to faults in the pressure signal cannot be accurately captured during the feature extraction process, the following classifiers tend to struggle to distinguish between normal and faulty states, thereby generating an unacceptable performance. In contrast, the flow rate signal and exergy signal are more suitable for leakage fault detection and diagnosis in pneumatic systems.

Furthermore, the classification performance of the pressure signal is quite different in the two experiments. In experiment II, the performance of the pressure signal slightly decreased across all classifiers compared to experiment I. This could be attributed to variations in operating conditions in experiments or differences in the data, such as changes in experimental conditions or alterations in sample distributions. Further research and analysis are required to determine the specific reasons behind these differences.

4.3. Comparison of Different Machine Learning Algorithms

From Figures 12 and 13, it is clear that the performance of the average accuracy of the three classifiers is very similar from the perspectives of different signals and different experiments. In general, SVM presents the highest average accuracy, followed by GPC and KNN. The average accuracy of KNN is slightly lower than SVM and GPC while it is still higher than 90% in terms of the flow rate signal and exergy signal. According to Tables 9 and 10, it is evident that similar trends are presented for three classifiers. The macro-precision, macro-recall, and macro-F1-score of the three classifiers are all almost 1 when the flow rate signal and exergy signal are investigated. Thus, based on the metrics of average accuracy, macro-precision, macro-recall, and macro-F1-score, the SVM performs the best with a slight advantage over GPC.

Tables 11 and 12 show the computational complexity of three classifiers in experiment I and experiment II, respectively. It is clear that the SVM shows the smallest storage space requirement, the shortest training time, and the shortest prediction time in both experiments compared with the KNN and GPC. The GPC presents a significantly larger storage space requirement, longer training time, and longer prediction time. It should be noted that the KNN does not have a specific training process as it is a "lazy learning" algorithm. Thus, there is no specific training time to record for KNN. Although the training time for the KNN classifier is not provided, it typically has a shorter prediction time. Shorter training and prediction times indicate higher efficiency for classifiers. Therefore, the SVM and KNN show acceptable computational complexity.

Table 11. Computational complexity of classifiers in experiment I.

Classifiers	Signal	Storage Capacity	Training Time	Prediction Time
GPC	Flow rate	234,476,835 bytes	916.48 s	1.32 s
	Pressure	234,476,835 bytes	985.17 s	1.09 s
	Exergy	234,476,774 bytes	803.98 s	1.08 s
SVM	Flow rate	51,732 bytes	0.031 s	0.031 s
	Pressure	85,656 bytes	0.035 s	0.012 s
	Exergy	50,036 bytes	0.034 s	0.0080 s
KNN	Flow rate	251,049 bytes	-	0.013 s
	Pressure	251,049 bytes	-	0.013 s
	Exergy	251,049 bytes	-	0.014 s

Table 12. Computational complexity of classifiers in experiment II.

Classifiers	Signal	Storage Capacity	Training Time	Prediction Time
GPC	Flow rate	234,476,835 bytes	646.31 s	1.46 s
	Pressure	234,476,835 bytes	1176.16 s	1.98 s
	Exergy	234,476,835 bytes	1103.60 s	3.41 s
SVM	Flow rate	42,192 bytes	0.17 s	0.0090 s
	Pressure	44,524 bytes	0.11 s	0.0060 s
	Exergy	51,520 bytes	0.11 s	0.0080 s
KNN	Flow rate	251,049 bytes	-	0.021 s
	Pressure	251,049 bytes	-	0.011 s
	Exergy	251,049 bytes	-	0.036 s

In summary, in this study, the SVM classifier outperforms the KNN and GPC classifiers when comprehensively considering the evaluation metrics. However, it should also be noted that the application of this conclusion should be limited. The analyses of average accuracy and computational complexity are based on the experimental data collected in experiments instead of practical industrial applications. The performance of classifiers in actual systems can be influenced by more complex factors such as dataset size, algorithm complexity, hardware constraints, and specific application requirements. When selecting classifiers for practical applications, considerations should go beyond storage space, training time, and prediction time. Other factors such as accuracy, macro-precision, macro-recall, macro-F1-score, interpretability, adaptability to dynamic environments, and the availability of sufficient training data should be taken into account. A careful evaluation of the trade-offs between different classifiers is necessary to determine the most suitable classifier for specific application needs.

5. Conclusions

In this study, the leakage faults of two parallel-installed pneumatic cylinders are detected and diagnosed with different signals and different machine learning methods. This study preliminarily solves the three issues proposed in the Introduction Section. The conclusions are drawn as follows.

- It is feasible to conduct fault diagnosis in pneumatic systems using a minimal number of low-cost sensors while ensuring high-precision results. In the context of this study, both experiments I and II achieve a maximum average fault diagnosis accuracy of 100%. With the help of machine learning methods, leakage faults were successfully diagnosed using data collected from a single measurement point upstream of the system.
- The exergy signal outperforms the flow rate signal and pressure signal in terms of accuracy, macro-precision, macro-recall, and macro-F1-score. Furthermore, the performance of exergy is insensitive to the operating conditions of the system and machine learning algorithms. When compared with the conventional flow rate and pressure signals, the exergy signal exhibited an increase in average accuracy ranging from 0.62% to 33.12%. Exergy combines the features of pressure and flow rate, thereby overcoming difficulties in signal selection and ensuring the diagnosis performance of leakage faults.
- Considering classification performance and computational complexity, the results of this study indicate that the SVM classifier is more suitable for this scenario. The SVM classifier requires about 1/4 and 1/5552 of the storage space of the GPC and KNN classifiers, respectively. The training time of SVM is approximately 1/3797 to 1/29,556 of that of the GPC classifier. Therefore, using the SVM classifier for similar pneumatic system fault diagnosis is recommended to achieve efficient and accurate fault diagnosis in terms of the scenario investigated in this study.

The above conclusions are significant for developing a low-cost intelligent fault diagnosis system for pneumatics. Although only two parallel-installed pneumatic cylinders are investigated in this study, the methodology could be applied to more complex pneumatic systems with more components and faults. This provides a preliminary verification for exploring and identifying a low-redundancy and low-cost monitoring sensor network in pneumatic systems.

Author Contributions: Conceptualization, Z.W. and W.X.; methodology, H.Z. and Z.W.; software, H.Z.; validation, H.Z., Z.W., H.W. and Z.Z.; formal analysis, H.Z. and Z.W.; investigation, H.Z., Z.W., H.W. and Z.Z.; writing—original draft preparation, H.Z. and Z.W.; writing—review and editing, Z.W. and W.X.; visualization, H.Z. and Z.W.; project administration, Z.W.; funding acquisition, Z.W. and W.X. All authors have read and agreed to the published version of the manuscript.

Funding: This research was funded by National Natural Science Foundation of China, grant number 51905066 and 52075065.

Data Availability Statement: The data presented in this study are available on request from the corresponding author.

Conflicts of Interest: The authors declare no conflict of interest.

References

1. Shi, Y.; Cai, M.; Xu, W.; Wang, Y. Methods to evaluate and measure power of pneumatic system and their applications. *Chin. J. Mech. Eng.* **2019**, *32*, 42. [CrossRef]
2. Qian, P.; Pu, C.; Liu, L.; Li, X.; Zhang, B.; Gu, Z.; Meng, D. Development of a new high-precision friction test platform and experimental study of friction characteristics for pneumatic cylinders. *Meas. Sci. Technol.* **2022**, *33*, 065001. [CrossRef]
3. Luo, W. Troubleshooting of Common Fault for Pneumatic System. *Chin. Hydraul. Pneum.* **2004**, *2*, 68–69.
4. Wang, X.; Gao, L.; Tao, G. Principles and experimental research of expert system for fault diagnosis of pneumatic production line. *Hydraul. Pneum. Seals* **2001**, *4*, 1–4.
5. Guo, B.; Qi, F.; Fu, G. A knowledge-based diagnostic system for pneumatic system. In Proceedings of the 2008 International Symposium on Knowledge Acquisition and Modeling, Wuhan, China, 21–22 December 2008; pp. 127–130.
6. Zhang, D.; Hao, J.; Chen, L.; Zhou, L. Fault Diagnosis Approach for Pneumatic Control Valves Based on Modified Expert System. In Proceedings of the 2020 19th International Symposium on Distributed Computing and Applications for Business Engineering and Science (DCABES), Xuzhou, China, 16–19 October 2020; pp. 104–107.
7. Barner, A.; Bredau, J.; Schiller, F. Efficient Drive-Based Analysis of Fault Detection Measures in Safety-Related Pneumatic Systems. In Proceedings of the Annual Conference of the PHM Society, Portland, OR, USA, 10–16 October 2010.
8. Zhao, F.; Tian, Z.; Zeng, Y. Uncertainty quantification in gear remaining useful life prediction through an integrated prognostics method. *IEEE Trans. Reliab.* **2013**, *62*, 146–159. [CrossRef]
9. Yang, X.; Ran, Y.; Zhang, G.; Wang, H.; Mu, Z.; Zhi, S. A digital twin-driven hybrid approach for the prediction of performance degradation in transmission unit of CNC machine tool. *Robot. Comput.-Integr. Manuf.* **2022**, *73*, 102230. [CrossRef]
10. Luo, W.; Hu, T.; Ye, Y.; Zhang, C.; Wei, Y. A hybrid predictive maintenance approach for CNC machine tool driven by Digital Twin. *Robot. Comput.-Integr. Manuf.* **2020**, *65*, 101974. [CrossRef]
11. Santolamazza, A.; Cesarotti, V.; Introna, V. Anomaly detection in energy consumption for Condition-Based maintenance of Compressed Air Generation systems: An approach based on artificial neural networks. *IFAC-PapersOnLine* **2018**, *51*, 1131–1136. [CrossRef]
12. Yin, J.; Zhu, L.; Yu, G.; Shao, Y.; Guan, H. Fault Diagnosis of Transformers Based on Gaussian Process Classifier. *Trans. China Electrotech. Soc.* **2013**, *28*, 158–164.
13. Qi, G.; Zhu, Z.; Erqinhu, K.; Chen, Y.; Chai, Y.; Sun, J. Fault-diagnosis for reciprocating compressors using big data and machine learning. *Simul. Model. Pract. Theory* **2018**, *80*, 104–127. [CrossRef]
14. Moosavian, A.; Ahmadi, H.; Tabatabaeefar, A.; Khazaee, M. Comparison of Two Classifiers; K-Nearest Neighbor and Artificial Neural Network, for Fault Diagnosis on a Main Engine Journal-Bearing. *Shock. Vib.* **2013**, *20*, 360236. [CrossRef]
15. Liu, W.; Zhang, Z.; Zhang, J.; Huang, H.; Zhang, G.; Peng, M. A Novel Fault Diagnosis Method of Rolling Bearings Combining Convolutional Neural Network and Transformer. *Electronics* **2023**, *12*, 1838. [CrossRef]
16. Bai, H.; Zhan, X.; Yan, H.; Wen, L.; Yan, Y.; Jia, X. Research on Diesel Engine Fault Diagnosis Method Based on Stacked Sparse Autoencoder and Support Vector Machine. *Electronics* **2022**, *11*, 2249. [CrossRef]
17. Borg, M.; Refalo, P.; Francalanza, E. Failure Detection Techniques on the Demand Side of Smart and Sustainable Compressed Air Systems: A Systematic Review. *Energies* **2023**, *16*, 3188. [CrossRef]
18. Feng, Z.; Yang, J. Research on Fault Diagnosis Algorithm of Self-validating Pneumatic Actuator. *Chin. J. Sens. Actuators* **2022**, *35*, 785–791.
19. Leu van, K.; Sun, Y.; Chen, L.; Fang, M.; Zhang, M. Research on Fault Diagnosis Method of Pneumatic Circuit Used Bidirectional LSTM Neural Network. *Comput. Digit. Eng.* **2022**, *50*, 367–372.
20. Kovacs, T.; Ko, A. Monitoring pneumatic actuators' behavior using real-world data set. *SN Comput. Sci.* **2020**, *1*, 196. [CrossRef]
21. Ertel, W.; Lehmann, R.; Medow, R.; Finkbeiner, M.; Meyer, A. Model Free Diagnosis of Pneumatic Systems using Machine Learning. In Proceedings of the 9th International Fluid Power Conference, Aachen, Germany, 24–26 March 2014.
22. Demetgul, M.; Tansel, I.N.; Taskin, S. Fault diagnosis of pneumatic systems with artificial neural network algorithms. *Expert Syst. Appl.* **2009**, *36*, 10512–10519. [CrossRef]
23. Li, X.; Kao, I. Analytical fault detection and diagnosis (FDD) for pneumatic systems in robotics and manufacturing automation. In Proceedings of the 2005 IEEE/RSJ International Conference on Intelligent Robots and Systems, Edmonton, AB, Canada, 2–6 August 2005; pp. 2517–2522.
24. Nagel, T.; Zhang, C.; Liu, S. Kalman filter based leak localization applied to pneumatic systems. In Proceedings of the 2012 12th International Conference on Control Automation Robotics & Vision (ICARCV), Guangzhou, China, 5–7 December 2012; pp. 1777–1782.
25. Dindorf, R.; Wos, P. Test of measurement device for the estimation of leakage flow rate in pneumatic pipeline systems. *Meas. Control.* **2018**, *51*, 514–527. [CrossRef]
26. Abela, K.; Refalo, P.; Francalanza, E. Analysis of pneumatic parameters to identify leakages and faults on the demand side of a compressed air system. *Clean. Eng. Technol.* **2022**, *6*, 100355. [CrossRef]
27. Shi, Y.; Chang, J.; Wang, Y.; Zhao, X.; Zhang, Q.; Yang, L. Gas Leakage Detection and Pressure Difference Identification by Asymmetric Differential Pressure Method. *Chin. J. Mech. Eng.* **2022**, *35*, 44. [CrossRef]
28. Tong, Z.; Wang, H.; Xiong, W.; Ting, D.S.K.; Carriveau, R.; Wang, Z. Accumulated and transient exergy analyses of pneumatic systems with isochoric and isobaric compressed air storage tanks. *Energy Storage* **2021**, *3*, e269. [CrossRef]

29. Shi, P.; Liang, K.; Zhao, N.; An, S. Intelligent gear fault diagnosis based on deep learning feature extraction and particle swarm support vector machine state recognition. *China Mech. Eng.* **2017**, *28*, 1056–1061.
30. Zhao, J.; Ren, S.; Chen, J.; Si, Q. Nonlinear System Modeling and Fault Diagnosis Method based on PRB-SAE Algorithm. *J. Eng. Therm. Energy Power* **2022**, *37*, 197–205.
31. Najafzadeh, M.; Tafarojnoruz, A. Evaluation of neuro-fuzzy GMDH-based particle swarm optimization to predict longitudinal dispersion coefficient in rivers. *Environ. Earth Sci.* **2016**, *75*, 157. [CrossRef]
32. Najafzadeh, M.; Tafarojnoruz, A.; Lim, S.Y. Prediction of local scour depth downstream of sluice gates using data-driven models. *ISH J. Hydraul. Eng.* **2017**, *23*, 195–202. [CrossRef]
33. Najafzadeh, M.; Rezaie-Balf, M.; Tafarojnoruz, A. Prediction of riprap stone size under overtopping flow using data-driven models. *Int. J. River Basin Manag.* **2018**, *16*, 505–512. [CrossRef]